J|A|C|S
ARTICLES
Published on Web 03/27/2007

# Tetrachelate Porphyrin Chromophores for Metal Oxide Semiconductor Sensitization: Effect of the Spacer Length and Anchoring Group Position

Jonathan Rochford,† Dorothy Chu,† Anders Hagfeldt,‡ and Elena Galoppini*,†

*Contribution from the Chemistry Department, Rutgers University, 73 Warren Street, Newark, New Jersey 07102, and Center of Molecular Devices, Department of Chemistry, Royal Institute of Technology, Teknikringen 30, SE 100 44 Stockholm, Sweden*

Received November 16, 2006; E-mail: galoppin@rutgers.edu

***Abstract:*** Four Zn(II)-tetra(carboxyphenyl)porphyrins in solution and bound to metal oxide ($TiO_2$, ZnO, and $ZrO_2$) nanoparticle films were studied to determine the effect of the spacer length and anchoring group position (para or meta) on their binding geometry and photoelectrochemical and photophysical properties. The properties of three types of anchoring groups (COOH and $COONHEt_3$) for four Zn(II)-porphyrins (Zn-(II)-5,10,15,20-tetra(4-carboxyphenyl)porphyrin (*p*-ZnTCPP), Zn(II)-5,10,15,20-tetra(3-carboxyphenyl)porphyrin (*m*-ZnTCPP), Zn(II)-5,10,15,20-tetra(3-(4-carboxyphenyl)phenyl)porphyrin (*m*-$ZnTCP_2P$), and Zn(II)-5,10,15,20-tetra(3-ethynyl(4-carboxyphenyl)phenyl)porphyrin (*m*-ZnTC(PEP)P)) were compared. In *m*-ZnTCPP, *m*-$ZnTCP_2P$, and *m*-ZnTC(PEP)P the four anchoring groups are in the meta position on the *meso*-phenyl rings of the porphyrin macrocycle, thus favoring a planar binding mode to the metal oxide surfaces. The three meta-substituted porphyrin salts have rigid spacer units of increasing length (phenyl (P), biphenyl ($P_2$), and diphenylethynyl (PEP)) between the porphyrin ring and the carboxy anchoring groups, thus raising the macrocycle from the metal oxide surface. All porphyrins studied here, when bound to $TiO_2$ and ZnO, exhibited quenching of the fluorescence emission, consistent with electron injection into the conduction band of the semiconductor. Steady-state UV−vis and fluorescence studies of *p*-ZnTCPP on insulating $ZrO_2$ showed evidence of aggregation and exciton coupling. This was not observed in any of the meta-substituted porphyrins. The photoelectrochemical properties (IPCE, $V_{oc}$, and $I_{sc}$) of the porphyrins bound to $TiO_2$ films in solar cells have been measured and rationalized with respect to the sensitizer binding geometry and distance from the surface.

## 1. Introduction

The investigation of semiconductor sensitization by organic and inorganic dyes for applications in dye-sensitized solar cells (DSSCs) is a very active area of research due to the need for efficient, environmentally friendly, and economically viable renewable energy sources.[1] One of the key requirements in the operation of this kind of solar cell is the sensitization of a wide band gap semiconductor, typically $TiO_2$ or ZnO, via electron injection from a photoexcited chromophore.[2] The efficiency of the electron-transfer step at the dye−semiconductor interface is highly dependent, among numerous other factors, on the way the chromophore is attached to the surface.[3] For instance, we, and others, have reported a series of "rigid-rod"[4,5] and "tripodal" linkers[6,7] to achieve some level of control over the orientation and distance of the sensitizer at the metal oxide surface. We have now designed and synthesized a series of tetra(carboxyphenyl)porphyrin derivatives (Figure 1) as models to determine how the distance and attachment of the sensitizing chromophore on colloidal $TiO_2$ and ZnO films influence interfacial processes and solar cell efficiencies. The interest in developing model

† Rutgers University.
‡ Royal Institute of Technology.

(1) (a) O'Regan, B.; Grätzel, M. *Nature* **1991**, *353*, 737. (b) Grätzel, M. *Nature* **2001**, *414*, 338. (c) Grätzel, M. *Inorg. Chem.* **2005**, *44*, 6841. (d) Kalyanasundaram, K.; Grätzel, M. *Coord. Chem. Rev.* **1998**, *177*, 347. (e) Kamat, P. V. *Chem. Rev.* **1993**, *93*, 267−300. (f) Qu, P.; Meyer, G. J. In *Electron Transfer in Chemistry*; Balzani, V., Ed.; John Wiley & Sons: New York, 2001; Vol. IV, Part 2, Chapter 2, pp 355−411.
(2) (a) Anderson, N. A.; Lian, T. *Coord. Chem. Rev.* **2004**, *248*, 1231. (b) Schwarzburg, K.; Ernstofer, R.; Felber, S.; Willig, F. *Coord. Chem. Rev.* **2004**, *248*, 1259. (c) Benkö, G.; Kallioinen, J.; Korppi-Tommola, J. E. I.; Yartsev, A.; Sundström, V. *J. Am. Chem. Soc.* **2002**, *124*, 489.
(3) (a) Clifford, J. N.; Palomares, E.; Nazeeruddin, Md. K.; Grätzel, M.; Nelson, J.; Li, X.; Long, N. J.; Durrant, J. R. *J. Am. Chem. Soc.* **2004**, *126*, 5225. (b) Palomares, E.; Martínez-Diaz, M. V.; Haque, S. A.; Torres, T.; Durrant, J. R. *Chem. Commun.* **2004**, *18*, 2112. (c) Durrant, J. R.; Haque, S. A.; Palomares, E. *Coord. Chem. Rev.* **2004**, *248*, 1247.
(4) (a) Hoertz, P. G.; Carlisle, R. A.; Meyer, G. J.; Wang, D.; Piotrowiak, P.; Galoppini, E. *Nano Lett.* **2003**, *3*, 325. (b) Wang, D.; Mendelsohn, R.; Galoppini, E.; Hoertz, P. G.; Carlisle, R. A.; Meyer, G. J. *J. Phys. Chem. B* **2004**, *108*, 16642. (c) Taratula, O.; Rochford, J.; Piotrowiak, P.; Galoppini, E.; Carlisle, R. A.; Meyer, G. J. *J. Phys. Chem. B* **2006**, *110*, 15734.
(5) Kilså, K.; Mayo, E. I.; Kuciauskas, D.; Villahermosa, R.; Lewis, N. S.; Winkler, J. R.; Gray, H. B. *J. Phys. Chem. A* **2003**, *107*, 3379.
(6) (a) Galoppini, E.; Guo, W.; Qu, P.; Meyer, G. J. *J. Am. Chem. Soc.* **2001**, *123*, 4342. (b) Galoppini, E.; Guo, W.; Zhang, W.; Hoertz, P.; Qu, P.; Meyer, G. J. *J. Am. Chem. Soc.* **2002**, *124*, 7801. (c) Piotrowiak, P.; Galoppini, E.; Wei, Q.; Meyer, G. J.; Wiewiór, P. *J. Am. Chem. Soc.* **2003**, *125*, 5278. (d) Clark, C. C.; Meyer, G. J.; Wei, Q.; Galoppini, E. *J. Phys. Chem. B* **2006**, *110*, 11044.
(7) (a) Loewe, R. S.; Ambroise, A.; Muthukumaran, K.; Padmaja, K.; Lysenko, A. B.; Mathur, G.; Li, Q.; Bocian, D. F.; Misra, V.; Lindsey, J. S. *J. Org. Chem.* **2004**, *69*, 1453. (b) Wei, L.; Padmaja, K.; Youngblood, W. J.; Lysenko, A. B.; Lindsey, J. S.; Bocian, D. F. *J. Org. Chem.* **2004**, *69*, 1461. (c) Long, B.; Nikitin, K.; Fitzmaurice, D. *J. Am. Chem. Soc.* **2003**, *125*, 5152.

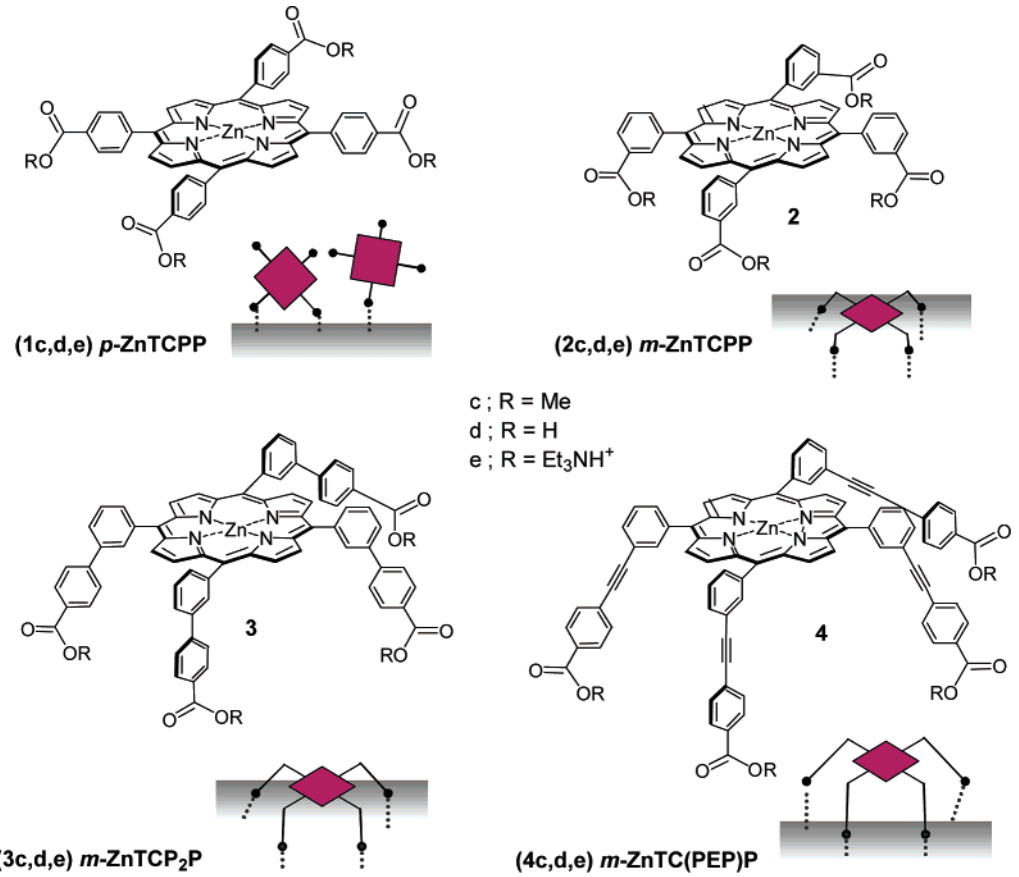


***Figure 1.*** Structures of the porphyrins employed in this study. Also shown are the anticipated binding geometries of the COOH and $COOEt_3NH$ derivatives on metal oxide surfaces. This diagram shows ideal behavior of the sensitizers on the metal oxide surface. However, we must assume that other binding modes are also likely. Due to the steric constraints of these systems it should take at least two of the four carboxy groups bound to the surface to fix the porphyrin chromophores in the rigid planar fashion depicted.

porphyrins was initiated by our electron transport study in a solar cell with the working electrode made of a ZnO nanowire film and sensitized with Zn(II)-5,10,15,20-tetra(3-carboxyphenyl)porphyrin (*m*-ZnTCPP).[8] Eventually, the compounds described here could be useful models to study interfacial processes in ZnO nanowire films.

In this paper we will discuss the synthesis, photophysical, electrochemical, and photoelectrochemical properties of the carboxylic acid derivatives (COOH, COOMe, and $COOEt_3NH$) of four tetrachelate Zn-porphyrins (Figure 1). Two (*m*-$ZnTCP_2P$ and *m*-ZnTC(PEP)P) are new compounds. For clarity, for all four porphyrins, the carboxylic acid derivatives are indicated with the suffix -[A] in the abbreviated name, the corresponding methyl esters with the suffix -[E], and the ammonium salts with the suffix -[S]. The carboxylic acid functionality is the most commonly used anchoring group for standard Grätzel-type DSSCs, and numerous DSSC devices employing carboxyporphyrins have been reported over the years.[1d,3a,c,9]

The presence of carboxy anchoring groups attached to the *meso*-phenyl ring of the porphyrin has little influence on the ground-state electronic nature of the dye, because of the orthogonal orientation of the *meso*-phenyl ring.[10] However, the *position* on the carboxylic acid anchoring groups on the *meso*-phenyl ring does have a great influence on the binding mode and, as a result, on other properties. For instance, Campbell et al. have reported a 5-fold increase in the short circuit photocurrent ($I_{sc}$) and a significantly higher open circuit photovoltage ($V_{oc}$) on changing the position of the COOH groups from the para (in *p*-ZnTCPP-[A]) to the meta position (in *m*-ZnTCPP-[A]).[9a] This effect was attributed to a more efficient electron injection from the meta porphyrin, which binds flat on the $TiO_2$ surface, compared to that of the para, which binds vertically (Figure 1).[9a,11] Our recent study of cells prepared from *m*-ZnTCPP-[A] bound to ZnO nanowires and ZnO colloidal

(8) Galoppini, E.; Rochford, J.; Chen, H.; Saraf, G.; Lu, Y.; Hagfeldt, A.; Boschloo, G. *J. Phys. Chem. B* **2006**, *110*, 16159.

(9) (a) Campbell, W. M.; Burrell, A. K.; Officer, D. L.; Jolley, K. W. *Coord. Chem. Rev.* **2004**, *248*, 1363 and references therein. (b) Argazzi, R.; Murakami Iha, N. Y.; Zabri, H.; Odobel, F.; Bignozzi, C. A. *Coord. Chem. Rev.* **2004**, *248*, 1299. (c) Nazeeruddin, M. K.; Humphry-Baker, R.; Officer, D. L.; Campbell, W. M.; Burrell, A. K.; Grätzel, M. *Langmuir* **2004**, *20*, 6514. (d) Watson, D. F.; Marton, A.; Stux, A. M.; Meyer, G. J. *J. Phys. Chem. B* **2004**, *108*, 11680. (e) Brune, A.; Jeong, G.; Liddell, P. A.; Sotomura, T.; Moore, T. A.; Moore, A. L.; Gust, D. *Langmuir* **2004**, *20*, 8366. (f) Jasieniak, J.; Johnston, M.; Waclawik, E. R. *J. Phys. Chem. B* **2004**, *108*, 12962. (g) Michaelis, E.; Nonomura, K.; Schlettwein, D.; Yoshida, T.; Minoura, H.; Wöhrle, D. *J. Porphyrins Phthalocyanines* **2004**, *12*, 1366. (h) Schmidt-Mende, L.; Campbell, W. M.; Wang, Q.; Jolley, K. W.; Officer, D. L.; Nazeeruddin, M. K.; Grätzel, M. *Chem. Phys. Chem.* **2005**, *6*, 1253. (i) Hasobe, T.; Hattori, S.; Kamat, P. V.; Urano, Y.; Umezawa, N.; Nagano, T.; Fukuzumi, S. *Chem. Phys.* **2005**, *319*, 243. (j) Wang, Q.; Campbell, W. M.; Bonfantani, E. E.; Jolley, K. W.; Officer, D. L.; Walsh, P. J.; Gordon, K.; Humphry-Baker, R.; Nazeeruddin, M. K.; Grätzel, M. *J. Phys. Chem. B* **2005**, *109*, 15397. (k) Hasobe, T.; Hattori, S.; Kamat, P. V.; Fukuzumi, S. *Tetrahedron* **2006**, *62*, 1937. (l) Lo, C.-F.; Luo, L.; Wei-Guang Diau, E.; Chang, I.-J.; Lin, C.-Y. *Chem. Commun.* **2006**, 1430. (m) Luo, L.; Lo, C.-F.; Lin, C.-Y.; Chang, I.-J.; Wei-Guang Diau, E. *J. Phys. Chem. B* **2006**, *110*, 410.

(10) (a) Schmidt, E. S.; Calderwood, T. S.; Bruice, T. C. *Inorg. Chem.* **1986**, *25*, 3718. (b) Seth, J.; Palaniappan, V.; Johnson, T. E.; Prathapan, S.; Lindsey, J. S.; Bocian, D. F. *J. Am. Chem. Soc.* **1994**, *116*, 10578. (c) Brückner, C.; Foss, P. C. D.; O' Sullivan, J.; Pelto, R.; Zeller, M.; Birge, R. R.; Crundwell, G. *Phys. Chem. Chem. Phys.* **2006**, *8*, 2402.

nanoparticle films motivated us to investigate such orientation effects further. In particular, we were interested to study the influence of both distance and binding geometry on the photophysical properties and solar cell efficiencies of the sensitizers.

## 2. Experimental Section

**2.1. Metal Oxide Film Preparation.** Colloidal $TiO_2$ and $ZrO_2$ films were prepared by a sol−gel technique that produces mesoporous films of approximately 10 $\mu$m thickness and that consist of nanoparticles with an average diameter of ∼20 nm (Supporting Information). ZnO films were prepared by a previously published method that produces mesoporous films of approximately 2 $\mu$m thickness with an average particle size of 15 nm.[12] Repeated depositions for making thicker ZnO films resulted in cracking and peeling of the film from the glass substrate. The $TiO_2$ films were prepared by casting the colloidal solutions by the doctor blade technique onto the substrate over an area of 1 × 2 $cm^2$, followed by sintering at ∼450 °C for 30 min. Lower temperatures were used for sintering the ZnO films (∼300−350 °C). For absorption and fluorescence studies the films were cast on cover glass slides (VWR). For electrochemical studies the films were cast on transparent, electronically conductive glass with an indium−tin−oxide layer (8 Ω/sq ITO, Pilkington). We will refer to films cast on cover glass or ITO conductive glass as MO/G or MO/ITO, respectively, where MO is the metal oxide. The preparation of the films for the solar cells employed in the photoelectrochemical studies followed slightly different procedures (see the Photoelectrochemistry section).

**2.2. Binding.** Binding of the dye molecules to the $TiO_2$, ZnO, and $ZrO_2$ films was accomplished by immersing the films in a 0.4 mM MeOH solution of the dye at room temperature for 1 h. Short binding times were chosen to prevent aggregation of the porphyrins at the metal oxide surfaces. Basic or acidic pretreatment of the metal oxide films was tested, but binding was found to occur best on untreated films. All films, which were stored in the air, were dried by heating to 150 °C for 30 min and cooled to 80 °C prior to immersion in the dye solution. The sensitized films were rinsed, immersed in MeOH to remove physisorbed dye, and then used for spectroscopic or electrochemical measurements. The amount of bound dye was estimated by calculating the amount of desorbed dye per gram of $TiO_2$ following a reported method.[13] This involved treating a combination of five films with 5 mL of 0.1 N NaOH(aq) and determining the average concentration per film of desorbed dye from the UV−vis absorption spectrum, using the extinction coefficient measured in basic solution. The five $TiO_2$ films (stripped of the dye) were then immersed in deionized water for 1 h, dried at 150 °C for 1 h, and the weight of $TiO_2$ on each glass slide was determined by scraping the films from the surface.

**2.3. Spectroscopy.** The FT-ATR-IR spectra of all porphyrins were measured neat (as powders) and bound to $TiO_2$ (Figures 2 and 3 and Supporting Information). Fourier transform infrared attenuated total reflectance (FT-IR-ATR) spectra were acquired on a Thermo Electron Corporation Nicolet 6700 FT-IR. UV−vis absorption spectra were acquired at ambient temperature in MeOH (Acros, spectroscopic grade) using a Hewlett-Packard 8453 diode array spectrometer. The sensitized MO/G films were placed diagonally in a 1 cm square quartz cuvette in air while recording spectra. Steady-state fluorescence spectra were acquired on a Spex Fluorolog that had been calibrated with a standard NIST tungsten−halogen lamp. Sensitized MO/G films were placed diagonally in a 1 cm square quartz cuvette. The excitation beam was

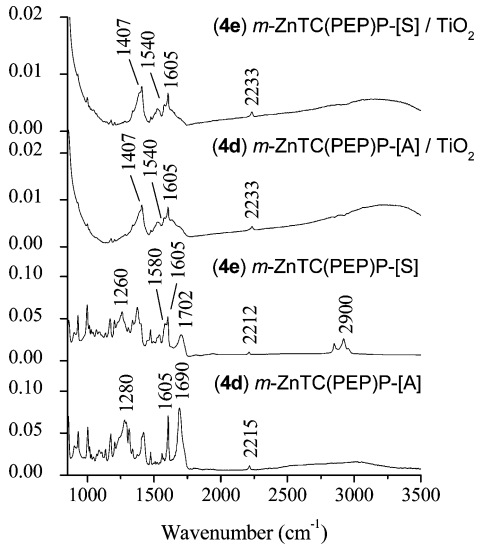


***Figure 2.*** FT-IR-ATR spectra of *m*-ZnTC(PEP)P solid and adsorbed on $TiO_2$ as the acid and the salt derivative. The broad bands observed at ∼3000 $cm^{-1}$ for the $TiO_2$ samples are assigned to adsorbed moisture on the films.

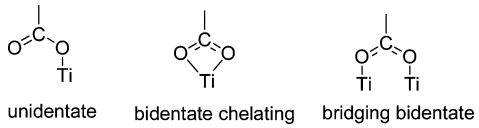


***Figure 3.*** Main binding modes of the carboxylate group to $TiO_2$.

directed 45° to the film surface, and the emitted light was monitored from the front face of the sample and from a 90° angle in the case of fluid solutions. Fluorescence quantum yields for the samples ($\Phi_{Fl}$) were calculated in MeOH solutions deareated by freeze−pump−thaw technique at $\lambda_{exc}$ = 565 nm, using the optically dilute technique with Zn(II)-5,10,15,20-tetraphenylporphyrin (ZnTPP) as the actinometer ($\Phi_{ref}$ = 0.033),[14] according to eq 1.

$$\Phi_{Fl} = (A_{ref}/A_s)(I_s/I_{ref})(\eta_s/\eta_{ref})^2\Phi_{ref} \quad (1)$$

The subscript "s" refers to the sample, the subscript "ref" to the reference sample (in this case ZnTPP), $A$ is the absorbance at the excitation wavelength, $I$ is the integrated emission area, and $\eta$ is the solvent refraction index.

**2.4. Electrochemistry.** Cyclic voltammetry was performed with a BAS potentiostat under nitrogen at room temperature with a conventional three-electrode configuration at a scan rate of 100 mV $s^{-1}$. The electrochemical properties of the methyl ester derivatives of the dyes were studied in dichloromethane with 0.1 M $Bu_4NBF_4$ supporting electrolyte. A glassy carbon working electrode (2 mm diameter) was used along with a platinum wire auxiliary electrode and a Ag/AgCl reference electrode. When using a porphyrin/MO/ITO film as the working electrode, acetonitrile was used with a 0.1 M $Bu_4NClO_4$ supporting electrolyte. In this case the porphyrins were bound as the tetra(triethylammonium)carboxyporphyrin salts. The potential of the Ag/AgCl electrode was calibrated externally versus the ferrocene/ferrocenium ($Fc^+$/Fc) redox couple. The half-wave redox potentials ($E_{1/2}$) were determined as $(E_{pa} + E_{pc})/2$, where $E_{pa}$ and $E_{pc}$ are the anodic and cathodic peak potentials, respectively. It was assumed that $E_{1/2} \cong E^{0\prime}$ for all measurements. All potentials were referenced to the normal hydrogen electrode (NHE) to make a comparison with the conduction bands of $TiO_2$ and ZnO. Where $E_{1/2}$ could not be calculated, due to irreversible oxidation or reduction processes, $E_{pa}$ and $E_{pc}$ were reported, respectively. All redox processes were also studied by differential pulse

(11) A similar comparison between meta- and para-substituted tetraphosphonic acid porphyrins bound to $TiO_2$ showed little change between the two structural isomers, see: Odobel, F.; Blart, E.; Lagrée, M.; Villieras, M.; Boujtita, H.; El Murr, N.; Caramori, S.; Bignozzi, C. A. *J. Mater. Chem.* **2003**, *13*, 502.

(12) Taratula, O.; Galoppini, E.; Wang, D.; Chu, D.; Zhang, Z.; Chen, H.; Saraf, G.; Lu, Y. *J. Phys. Chem. B* **2006**, *110*, 6506.

(13) Dabestani, R.; Bard, A. J.; Campion, A.; Fox, M. A.; Mallouk, T. E.; Webber, S. E.; White, J. M. *J. Phys. Chem.* **1988**, *92*, 1872.

(14) Strachan, J. P.; Gentemann, S.; Seth, J.; Kalsbeck, W. A.; Lindsey, J. S.; Holten, D.; Bocian, D. F. *J. Am. Chem. Soc.* **1997**, *119*, 11191.

voltammetry (DPV), using relationship 2

$$E_{1/2} = E_{max} + \Delta E/2 \quad (2)$$

where $E_{max}$ is the peak maxima in the DPV scan and $\Delta E$ is the pulse amplitude.[15] DPV experiments were carried out at a scan rate of 20 mV $s^{-1}$, pulse amplitude 50 mV, pulse width 50 mV, and pulse period 0.2 s. In some cases, namely, the third reduction process of some of the porphyrin dyes, the differential pulse voltammetry data are reported, due to poor quality cyclic voltammetry scans at such negative potentials.

The excited-state oxidation potentials $E_{1/2}(P^+/P^*)$ of all tetra(triethylammonium)carboxyporphyrins in methanol and bound to $TiO_2$ and ZnO surfaces were calculated from relationship 3

$$E_{1/2}(P^+/P^*) = E_{1/2}(P^+/P) - E_{0-0} \quad (3)$$

where $E_{1/2}(P^+/P)$ is equivalent to the first oxidation potential of the ground-state porphyrin chromophore and $E_{0-0}$ is the zero−zero excitation energy.[16] $E_{0-0}$ was calculated from the intersection of the porphyrin absorption spectrum with the fluorescence emission spectrum in methanol at normalized absorption/emission intensity. For the solid-state measurements $E_{0-0}$ was similarly calculated from the UV−vis and fluorescence measurements made on the derivatized MO/G and $ZrO_2$/G films, respectively. $E_{1/2}(P^+/P^*)$ values were calculated from the solid-state cyclic voltammetry, UV−vis, and fluorescence data to give a closer approximation of $E_{1/2}(P^+/P^*)$ in a solid-state device as possible.

**2.5. Photoelectrochemistry.** The $TiO_2$/FTO working electrodes for photoelectrochemical measurements were prepared by conventional methods. Briefly, a sample of EPFL B $TiO_2$ (Solaronics) was spread by the doctor blade technique over a 0.4 × 0.8 $cm^2$ area on a 1.5 × 1.5 $cm^2$ fluorine-doped tin−oxide (FTO) conductive glass electrode (Libby Owens Ford, 8 Ω/sq). The film was dried on a hot plate at 150 °C for 6 min, then sintered at 400 °C for 30 min. The films were cooled to ∼80 °C and then immediately immersed in the dye solutions (0.4 mM in MeOH). The films thus prepared were ∼10 μm thick (average), typically after two depositions. The Pt/FTO counterelectrode was prepared by depositing 15 μL of $H_2PtCl_6$ (5 mM in 2-propanol, Sigma-Aldrich) onto the conductive side of a 1.5 × 1.5 $cm^2$ FTO electrode followed by sintering for 30 min at 380 °C. An open cell set up was used, where a porous piece of lens paper tissue, wet with electrolyte (0.05 M $I_2$, 0.10 M LiI, 0.6 M TBAI in 3-methoxypropionitrile) was sandwiched between the sensitized $TiO_2$/FTO working electrode and the Pt/FTO counter electrode. All measurements were carried out under full sun conditions (1000 W $m^{-2}$) using an apparatus described previously.[17] The incident monochromatic photon-to-current conversion efficiency (IPCE) is plotted as a function of excitation wavelength according to equation (4)

$$\%IPCE(\lambda) = \frac{1240 I_{sc}}{\lambda \phi} \times 100 \quad (4)$$

where $I_{sc}$ is the photocurrent density (A $cm^{-2}$), $\lambda$ is the monitoring wavelength, and $\phi$ is the incident photon flux (W $cm^{-2}$).

**2.6. Synthesis 2.6.1. General.** All reactions involving air- and moisture-sensitive reagents were performed under nitrogen atmosphere in oven-dried or flame-dried glassware. A magnetic stirrer was used in all cases. Reagents were purchased from Fisher-Acros or Sigma-Aldrich Chemical Co. Benzaldehyde, methyl-4-iodobenzoate, methylbenzoate-4-carboxaldehyde, methylbenzoate-3-carboxaldehyde, methyl-4(3-formylphenyl)benzoate, trimethylsilylacetylene, 2,3-dichloro-5,6-dicyanoquinone (DDQ), tetrakis(triphenylphosphine)palladium(0), dichlorobis(triphenylphosphine)palladium(II), cuprous(I) iodide, zinc(II) acetate, sodium hydroxide, sodium bicarbonate, potassium carbonate, and tetrabutylammonium fluoride were all used as received. Ethyl acetate was purchased as HPLC grade and used as received. Pyrrole was freshly distilled under vacuum and over potassium hydroxide. Anhydrous tetrahydrofuran (THF) was distilled under nitrogen atmosphere from sodium/benzophenone immediately prior to use. Dichloromethane and hexane were distilled over $CaCl_2$ prior to use. Triethylamine and diisopropylamine were both distilled over $CaH_2$ prior to use. Column chromatography was performed using 230−600 mesh silica gel (Sorbent Technologies). Thin-layer chromatography (TLC) was carried out using silica gel plates with a fluorescent indicator (Sorbent Technologies) and UV as the detection method. High- and low-resolution mass spectra were collected at a commercial facility. NMR spectra were recorded on a Varian INOVA-500 spectrometer at 499.896 MHz for $^1H$ and 125.711 MHz for $^{13}C$ under ambient probe temperature using $CDCl_3$, $CD_3OD$, or THF-$d_8$ as solvent. Chemical shifts ($\delta$) are given in parts million (ppm) and reported to a precision of ±0.01 ppm for proton and carbon. Proton coupling constants ($J$) are given in Hertz (Hz) and reported to a precision of ±0.1 Hz. The spectra of all compounds were referenced to the residual solvent peak, i.e., $CHCl_3$ at 7.27 ppm and $CH_3OH$ at 4.87 ppm, for the $^1H$ spectra and were referenced to $CDCl_3$ at 77.00 ppm for all $^{13}C$ spectra. Satisfactory $^{13}C$ spectra for compounds *m*-$H_2$TCP$_2$P-[E], *m*-$H_2$TC(PEP)P-[E], *m*-ZnTCP$_2$P-[A], *m*-ZnTC(PEP)P-[A], *p*-ZnTCPP-[S], *m*-ZnTCPP-[S], *m*-ZnTCP$_2$P-[S], and *m*-ZnTC(PEP)P-[S] could not be obtained because of their poor solubility. Mass spectrometry analysis (FAB) of all tetra(triethylammonium)carboxyporphyrin salts only showed molecular ions of the carboxylic acid derivatives due to formation of the acids in the matrix. UV−vis absorption spectra were collected on a Varian Cary-500 spectrometer using spectrophotometric grade solvents. 3-Ethynylbenzaldehyde was synthesized by following a published procedure.[18] Porphyrins *p*-$H_2$TCPP-[E],[19] *m*-$H_2$TCPP-[E],[20] *p*-ZnTCPP-[E],[19] *m*-ZnTCPP-[E], [20] *p*-ZnTCPP-[A],[19] and *m*-ZnTCPP-[A][9a] have been previously reported using a similar synthetic methodology. However, $^1H$ NMR spectra were not always published and are therefore included in the Supporting Information.

**2.6.2. Methyl-4(ethynyl-3-formylphenyl)benzoate (4a).** A flask was charged with methyl-4-iodobenzoate 0.79 g (3 mmol) and 3-ethynylbenzaldehyde (0.39 g, 3 mmol) followed by dichlorobis(triphenylphosphine)palladium(II) (68 mg, 0.06 mmol, 2% equiv) and CuI (11 mg, 0.06 mmol, 2% equiv) under nitrogen. Triethylamine (5 mL) was then added to the reaction flask via syringe. The reaction mixture was stirred for 24 h at room temperature and then poured into 10 mL of water. The product was extracted with ethyl acetate (10 mL), and the organic layer was washed repeatedly with water to remove any residual amine. The organic phase was dried over $NaSO_4$, and the solvent was removed in vacuo. The crude product was purified by silica gel flash chromatography using dichloromethane/ethyl acetate (1:1) to afford of a pale yellow solid (547 mg, 2.07 mmol, yield 69%): $R_f = 0.58$. $^1H$ NMR $\delta_H$ ($CDCl_3$): 10.04 (s, 1H), 8.06 (m, 3H), 7.88 (d, 1H, $J = 7.0$ Hz), 7.79 (d, 1H, $J = 7.0$ Hz)), 7.63 (d, 2H, $J = 9.0$ Hz), 7.56 (dd, 1H, $J = 8.0$ Hz) ppm. $^{13}C$ NMR $\delta_C$ ($CDCl_3$): 191.36, 166.44, 162.40,137.05, 136.59, 133.03, 131.62, 129.91, 129.60, 129.40, 129.22, 127.48, 124.04, 90.62, 90.06, 52.27 ppm. FT-IR-ATR: $\upsilon$(C═O) 1716, 1695 $cm^{-1}$; $\upsilon$(C−O) 1279 $cm^{-1}$. LRMS (FAB): $m/z$ 265.3 [$MH^+$].

**2.6.3. General Procedure for the Preparation of Tetramethylbenzoate Porphyrins.** Compounds **3b** *m*-$H_2$TCP$_2$P-[E] and **4b** *m*-$H_2$TC(PEP)P-[E] were prepared following the two-step one-flask room-temperature procedure that is used for the synthesis of meso-substituted

(15) Bard, A. J.; Faulkner, L. R. In *Electrochemical Methods: Fundamentals and Applications*, 2nd ed.; Wiley: New York, 2001.
(16) Kuciauskus, D.; Monat, J. E.; Villahermosa, R.; Gray, H. B.; Lewis, N. S.; McCusker, J. K. *J. Phys. Chem. B* **2002**, *106*, 9347.
(17) Lindström, H.; Magnusson, E.; Holmberg, A.; Södergren, S.; Lindquist, S.-E.; Hagfeldt, A. *Sol. Energy Mater. Sol. Cells* **2002**, *73*, 91.
(18) Vicente, M. G. H.; Shetty, S. J.; Wickramashinge, A.; Smith, K. M. *Tetrahedron Lett.* **2000**, *41*, 7623.
(19) Koehorst, R. B. M.; Boschloo, G. K.; Savenije, T. J.; Goosens, A.; Schaafsma, T. J. *J. Phys. Chem. B* **2000**, *104*, 2371.
(20) Bonar-Law, R. P.; Sanders, J. K. M. *J. Chem. Soc., Perkin Trans. 1* **1995**, 3085.

***Scheme 1.*** Synthetic Strategy Followed for the Preparation of the Porphyrin Sensitizers[a]

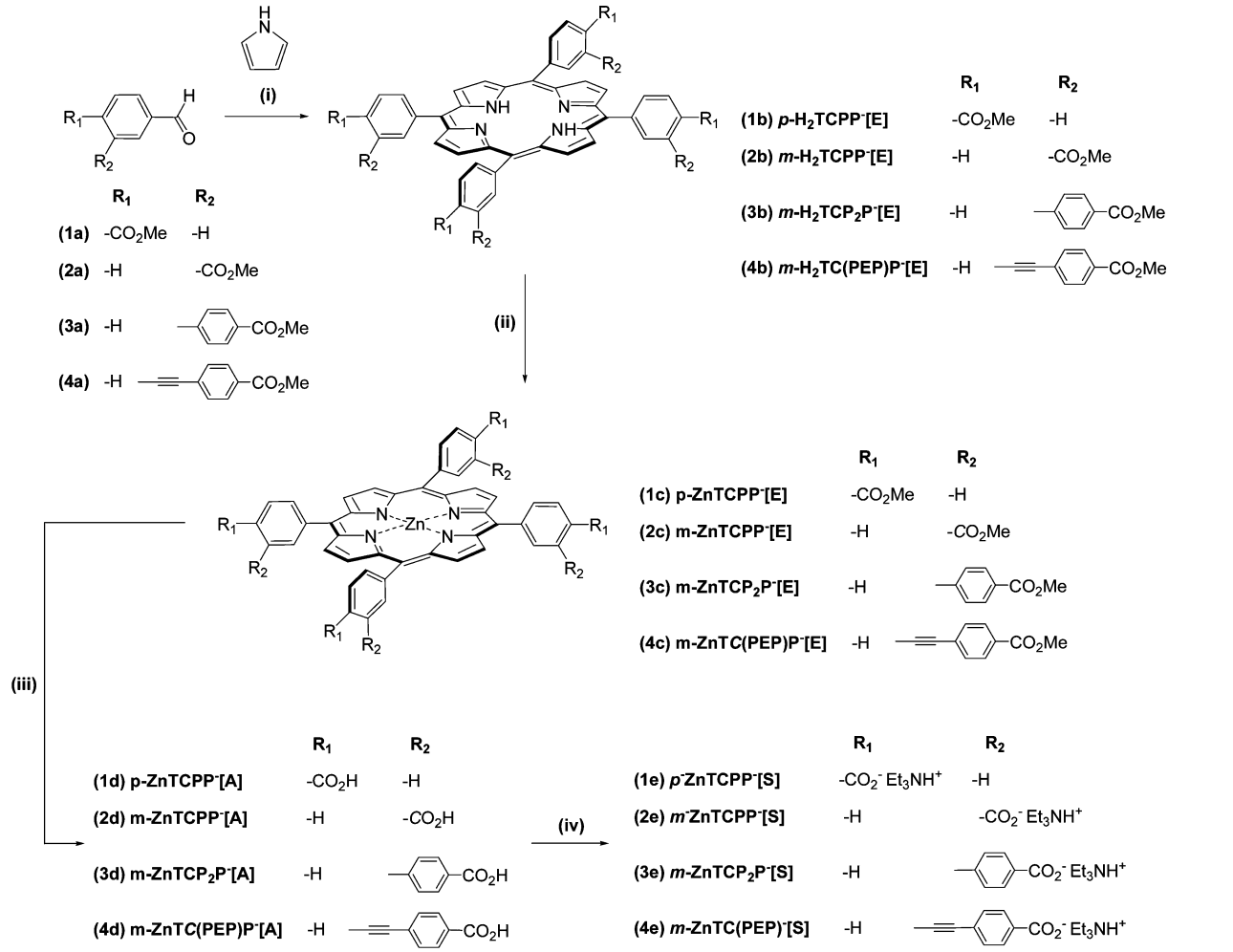


[a] Reagents and conditions: (i) $CH_2Cl_2$/TFA/DDQ, $N_2$/room temperature/12 h, 22−30% yield; (ii) $Zn(OAc)_2$/$CH_2Cl_2$/MeOH, room temperature/12 h, 86−92% yield; (iii) 2 N aqueous NaOH/THF, room temperature/3 days, 68−82% yield; (iv) $Et_3N$/THF/EtOAc, room temperature/3 h, 68−76% yield.

***Scheme 2.*** Synthesis of **4a**

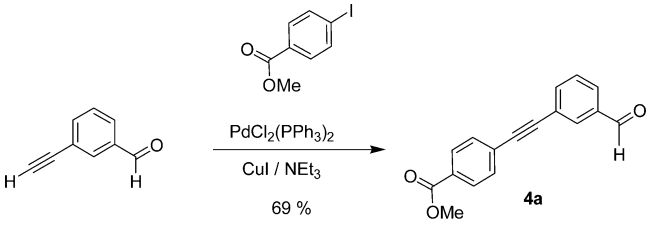


porphyrins.[21] Pyrrole (175 $\mu$L, 2.5 mmol) and the aldehydes **3a** and **4a**, respectively, 2.5 mmol) were dissolved in $CH_2Cl_2$ (100 mL) and the solution was purged with nitrogen for 10 min. The reaction mixture was then treated with trifluoroacetic acid (186 $\mu$L, 2.5 mmol) and stirred overnight (12 h) at room temperature, resulting in a deep red solution. DDQ (425 mg, 1.88 mmol) was then added to the solution in one portion, and stirring was continued for 6 h. $NaHCO_3$ (∼5 g) was then added in one portion to the reaction mixture, which was stirred until the acid was neutralized. After gravity filtration, the solvent was evaporated and the crude mixture was purified by silica gel gravity chromatography using dichloromethane/ethyl acetate (95:5) to afford pure porphyrin.

**2.6.4. $H_2$-5,10,15,20-tetra(3-(4-methylbenzoate)phenyl)porphyrin (3b, *m*-$H_2$TCP$_2$P-[E]).** $R_f$ = 0.59; yield: 198 mg (0.17 mmol; 28%). $^1$H NMR $\delta_H(CDCl_3)$: 8.95 (s, 8H), 8.53 (m, 4H), 8.30 (d, 4H, $J$ = 7.5), 8.15 (d, 8H, $J$ = 8.5), 8.07 (d, 4H, $J$ = 7.5), 7.93 (m, 12H), 3.94 (s, 12H), −2.70 (s, 2H) ppm. FT-IR-ATR: $\upsilon$(C═O) 1728 cm$^{-1}$; $\upsilon$(C−O) 1269 cm$^{-1}$. LRMS (FAB): $m/z$ 1151.3 [MH$^+$]. UV−vis $\lambda_{max}$ (MeOH): 421, 516, 549, 594, 654 nm.

**2.6.5. $H_2$-5,10,15,20-tetra(3-ethynyl(4-methylbenzoate)phenyl)-porphyrin (4b, *m*-$H_2$TC(PEP)P-[E]).** $R_f$ = 0.65; yield: 175 mg (0.14 mmol; 22%). $^1$H NMR $\delta_H(CDCl_3)$: 8.91 (s, 8H), 8.44 (m, 4H), 8.25 (d, 4H, $J$ = 7.5), 8.01 (m, 12H), 7.79 (t, 4H, $J$ = 7.5), 7.64 (d, 4H, $J$ = 8.0), 3.92 (s, 12H), −2.80 (s, 2H) ppm. FT-IR-ATR: $\upsilon$(C═O) 1727 cm$^{-1}$; $\upsilon$(C−O) 1267 cm$^{-1}$. LRMS (FAB): $m/z$ 1247.3 [MH$^+$]. UV−vis $\lambda_{max}$ (MeOH): 420, 515, 548, 591, 653 nm.

**2.6.6. General Procedure for Porphyrin Metalation.** The free base porphyrin (0.10 mmol) was dissolved in $CH_2Cl_2$ (20 mL), and the solution was purged with nitrogen for 10 min. A solution of $Zn(OAc)_2$ (32 mg, 0.15 mmol) in MeOH (5 mL) was added to the porphyrin solution in one portion, and the reaction mixture was stirred overnight (12 h). The solvents were removed in vacuo leaving a purple solid, which was dissolved in $CH_2Cl_2$ and washed successively with 5% aqueous $NaHCO_3$ and water. The organic layer was dried over $MgSO_4$, and the solvent was removed in vacuo. The metalloporphyrins were obtained in excellent (close to quantitative) yields following silica gel chromatography with dichloromethane/ethyl acetate (95:5).

**2.6.7. Zn(II)-5,10,15,20-tetra(3-(4-methylbenzoate)phenyl)porphyrin (3c, *m*-ZnTCP$_2$P-[E]).** $R_f$ = 0.60; yield: 108 mg (0.089 mmol; 89%). $^1$H NMR $\delta_H(CDCl_3)$: 9.05 (s, 8H), 8.51 (m, 4H), 8.30 (m, 4H), 8.05 (m, 12H), 7.88 (m, 12H), 3.85 (s, 12H) ppm. $^{13}$C NMR

(21) Lindsey, J. S.; Schreiman, I. C.; Hsu, H. C.; Kearney, P.; Marguerettaz, A. M. *J. Org. Chem.* **1987**, *52*, 827.

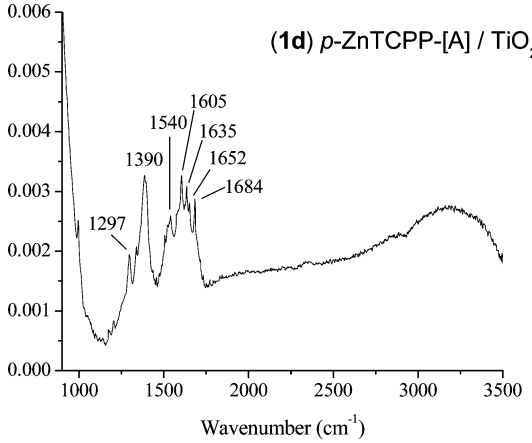


***Figure 4.*** FT-IR-ATR spectra of *p*-ZnTCPP-A bound to $TiO_2$. The broad bands observed at ~3000 $cm^{-1}$ for the $TiO_2$ samples are assigned to adsorbed moisture on the film.

$\delta_C(CDCl_3)$: 166.81, 150.23, 145.25, 143.41, 138.08, 134.12, 133.25, 132.17, 130.12, 128.87, 127.27, 127.19, 126.40, 120.80 ppm. FT-IR-ATR: $\upsilon$(C═O) 1722 $cm^{-1}$; $\upsilon$(C−O) 1275 $cm^{-1}$. HRMS (MALDI): *m*/*z* 1212.3140 [$M^+$]. Calcd for $C_{76}H_{52}N_4O_8Zn$: 1212.3077. UV−vis $\lambda_{max}$ (MeOH): 426, 557, 596 nm.

**2.6.8. Zn(II)-5,10,15,20-tetra(3-ethynyl(4-methylbenzoate)phenyl)porphyrin (4c, *m*-ZnTC(PEP)P-[E]).** $R_f$ = 0.65; yield: 121 mg (0.092 mmol; 92%). $^1$H NMR $\delta_H(CDCl_3)$: 9.00 (s, 8H), 8.43 (m, 4H), 8.24 (d, 4H, *J* = 7.5), 7.97 (d, 4H, *J* = 8.5), 7.91 (m, 8H), 7.78 (t, 4H, *J* = 7.5), 7.57 (m, 8H), 3.86 (s, 12H) ppm. $^{13}$C NMR $\delta_C(CDCl_3)$: 166.22, 150.06, 143.04, 137.26, 134.61, 132.07, 131.29, 131.27, 130.94, 129.25, 129.23, 129.11, 129.09, 127.62, 127.60, 126.77, 121.09, 120.00, 92.38, 88.72 ppm. FT-IR-ATR: $\upsilon$(C═O) 1720 $cm^{-1}$; $\upsilon$(C−O) 1270 $cm^{-1}$. HRMS (FAB): *m*/*z* 1308.3088 [$M^+$]. Calcd for $C_{84}H_{52}N_4O_8Zn$: 1308.3077. UV−vis $\lambda_{max}$ (MeOH): 425, 557, 597 nm.

**2.6.9. General Procedure for Hydrolysis of the Porphyrins Esters to Acids.** The porphyrin tetramethyl ester (0.10 mmol) was dissolved in THF (10 mL), and 2 N NaOH(aq) (5 mL) was then added in one portion. The solution was stirred at room temperature for 3 days. The THF was removed in vacuo, and any unreacted ester was extracted with chloroform. The acid was precipitated by the slow addition of 1 N HCl(aq) to the aqueous phase. The precipitate was filtered and thoroughly washed with water and diethyl ether.

**2.6.10. Zn(II)-5,10,15,20-tetra(3-(4-carboxyphenyl)phenyl)porphyrin (3d, *m*-ZnTCP$_2$P-[A]).** Yield: 95 mg (0.082 mmol; 82%). $^1$H NMR $\delta_H$(THF-$d_8$): 8.97 (s, 8H), 8.59 (m, 4H), 8.27 (m, 4H), 8.12 (m, 12H), 8.00 (m, 8H), 7.88 (m, 4H) ppm. FT-IR-ATR: $\upsilon$(C═O) 1686 $cm^{-1}$; $\upsilon$(C−O) 1283 $cm^{-1}$. HRMS (FAB): *m*/*z* 1157.2516 [$MH^+$]. Calcd for $C_{72}H_{45}N_4O_8Zn$: 1157.2529. UV−vis $\lambda_{max}$ (MeOH): 424, 557, 596 nm.

**2.6.11. Zn(II)-5,10,15,20-tetra(3-ethynyl(4-carboxyphenyl)phenyl)porphyrin (4d, *m*-ZnTC(PEP)P-[A]).** Yield: 99 mg (0.079 mmol; 79%). $^1$H NMR $\delta_H(CD_3OD)$: 8.92 (s, 8H), 8.43 (m, 4H), 8.28 (m, 4H), 7.98 (m, 12H), 7.81 (m, 4H), 7.62 (m, 8H) ppm. FT-IR-ATR: $\upsilon$(C═O) 1690 $cm^{-1}$; $\upsilon$(C−O) 1280 $cm^{-1}$. HRMS (FAB): *m*/*z* 1252.2426 [$M^+$]. Calcd for $C_{80}H_{44}N_4O_8Zn$: 1252.2451. UV−vis $\lambda_{max}$ (MeOH): 425, 557, 597 nm.

**2.6.12. General Procedure for the Synthesis of Porphyrin Tetra-(triethylammonium) Salts.** The porphyrin tetracarboxylic acid (0.05 mmol) was dissolved/suspended in THF (10 mL). $Et_3N$ (2−3 drops) was then added, and the solution was stirred at room temperature for 3 h. EtOAc (10 mL) was then added, and the THF was carefully removed under vacuum, leaving the higher boiling EtOAc behind. As the THF was removed, the porphyrin tetratriethylammonium salt precipitated out of solution. The purple solid was filtered and washed with EtOAc.[22]

**2.6.13. Zn(II)-5,10,15,20-tetra(4-triethylammoniumcarboxyphenyl)porphyrin (1e, *p*-ZnTCPP-[S]).** Yield: 48 mg (0.038 mmol; 76%). $^1$H NMR $\delta_H(CD_3OD)$: 8.84 (s, 8H), 8.34 (m, 8H), 8.22 (m, 8H), 3.02 (m, 24H), 1.20 (m, 36H) ppm. UV−vis $\lambda_{max}$ (MeOH): 424, 557, 597 nm. FT-IR-ATR: $\upsilon(CO_2^-)_{as}$ 1564 $cm^{-1}$; $\upsilon(CO_2^-)_s$ 1271 $cm^{-1}$.

**2.6.14. Zn(II)-5,10,15,20-tetra(3-triethylammoniumcarboxyphenyl)porphyrin (2e, *m*-ZnTCPP-[S]).** Yield: 44 mg (0.036 mmol; 71%). $^1$H NMR $\delta_H(CD_3OD)$: 8.80 (m, 12H), 8.39 (m, 8H), 7.81 (t, 4H, *J* = 7.5 Hz) ppm. UV−vis $\lambda_{max}$ (MeOH): 423, 558, 597 nm. FT-IR-ATR: $\upsilon(CO_2^-)_{as}$ 1564 $cm^{-1}$; $\upsilon(CO_2^-)_s$ 1271 $cm^{-1}$.

**2.6.15. Zn(II)-5,10,15,20-tetra(3-(4-triethylammoniumcarboxyphenyl)phenyl)porphyrin (3e, *m*-ZnTCP$_2$P-[S]).** Yield: 56 mg (0.036 mmol; 71%). $^1$H NMR $\delta_H(CD_3OD)$: 8.92 (s, 8H), 8.50 (m, 4H), 8.23 (m, 4H), 8.08 (m, 12H), 7.93 (d, 8H, *J* = 8.5 Hz), 7.85 (t, 4H, *J* = 7.5 Hz), 3.21 (m, 24H), 1.24 (m, 36H) ppm. UV−vis $\lambda_{max}$ (MeOH): 424, 558, 597 nm. FT-IR-ATR: $\upsilon(CO_2^-)_{as}$ 1580 (br) $cm^{-1}$; $\upsilon(CO_2^-)_s$ 1260 (br) $cm^{-1}$.

**2.6.16. Zn(II)-5,10,15,20-tetra(3-ethynyl(4-triethylammoniumcarboxyphenyl)phenyl)porphyrin (4e, *m*-ZnTC(PEP)P-[S]).** Yield: 56 mg (0.034 mmol; 68%). $^1$H NMR $\delta_H(CD_3OD)$: 8.88 (s, 8H), 8.35 (m, 4H), 8.20 (m, 4H), 7.92 (m, 12H), 7.78 (m, 4H), 7.56 (d, 8H, *J* = 7.5 Hz), 3.07 (m, 24H), 1.21 (m, 36H) ppm. UV−vis $\lambda_{max}$ (MeOH): 425, 558, 598 nm. FT-IR-ATR: $\upsilon(CO_2^-)_{as}$ 1580 (br) $cm^{-1}$; $\upsilon(CO_2^-)_s$ 1260 (br) $cm^{-1}$.

## 3. Results and Discussion

**3.1. Synthesis.** All porphyrins in this study were prepared using reported synthetic methodologies. First, the respective aldehydes were condensed with pyrrole using trifluoroacetic acid and 2,3-dichloro-5,6-dicyanoquinone (DDQ) as the oxidizing agent to form the tetra(methylbenzoate) porphyrin (Scheme 1).[21] After metalation upon reaction with $Zn(OAc)_2$, the four methyl ester groups were hydrolyzed in basic conditions to give the tetracarboxylic acid porphyrins. Porphyrins *p*-ZnTCPP-[A][19] and *m*-ZnTCPP-[A][9a] are known compounds and were synthesized in total yields of ~19% using methyl-4-formylbenzoate (**1a**) and methyl-3-formylbenzoate (**2a**), respectively. The synthesis of porphyrins *m*-ZnTCP$_2$P-[E] and *m*-ZnTC(PEP)P-[E] was performed using methyl-4-(3-formylphenyl)benzoate (**3a**) and methyl-4-(3-ethynylformylphenyl)benzoate (**4a**), respectively. **4a** was synthesized in 69% yield via the Sonogashira coupling reaction of 3-ethynylbenzaldehyde with methyl-4-iodobenzoate (Scheme 2). Both aldehydes undergo efficient porphyrin formation when condensed with pyrrole under the above conditions with total yields of 20% and 16% for *m*-ZnTCP$_2$P-[E] and *m*-ZnTC(PEP)P-[E], respectively. Porphyrin *m*-ZnTCP$_2$P-[A] was much less soluble in any solvent than *p*-ZnTCPP-[A], *m*-ZnTCPP-[A], and *m*-ZnTC(PEP)-[A]. To work with compounds that were equally soluble in the same solvents, the tetra-(triethylammonium)salts were readily prepared from the corresponding carboxylic acids using a small excess of triethylamine with yields of 68−76%.

**3.2. FT-IR-ATR. 3.2.1. Neat Samples.** All solid samples (Figure 2 and Supporting Information) showed spectra typical of the *meso*-tetraphenylporphyrin macrocycle with bands from the pyrrole C−H, C═C, and C═N stretches evident over the

(22) During the FAB-MS analysis of all tetrabutylammonium salts it was observed that all compounds were converted to their tetraacid precursors in the 3-nitrobenzyl alcohol/glycerol matrix.

***Table 1.*** Solution UV−Vis Absorption and Fluorescence Emission Data of $COOEt_3NH$ Derivatives of All Four Porphyrins in Methanol

| | UV−vis absorption | | | fluorescence |
|---|---|---|---|---|
| porphyrin | Soret $\lambda_{max}$, nm ($\epsilon \times 10^5$, $M^{-1}$ $L^{-1}$) | Q(1,0) $\lambda_{max}$, nm ($\epsilon \times 10^4$, $M^{-1}$ $L^{-1}$) | Q(0,0) $\lambda_{max}$, nm ($\epsilon \times 10^4$, $M^{-1}L^{-1}$) | $\lambda_{max}$, nm ($\Phi$) |
| (1e) *p*-ZnTCPP-[S] | 424 (2.78) | 557 (1.39) | 597 (0.53) | 606, 658 (0.023) |
| (2e) *m*-ZnTCPP-[S] | 423 (4.44) | 558 (2.09) | 597 (0.66) | 604, 657 (0.016) |
| (3e) *m*-ZnTCP2P-[S] | 424 (5.51) | 558 (2.77) | 597 (0.96) | 605, 659 (0.017) |
| (4e) *m*-ZnTC(PEP)P-[S] | 425 (5.93) | 558 (2.63) | 598 (0.83) | 604, 659 (0.018) |

range of 700−1500 $cm^{-1}$.[23] Neat samples of *m*-ZnTCPP-[A], *m*-$ZnTCP_2P$-[A], and *m*-ZnTC(PEP)P-[A] showed a strong band in the region of 1680−1690 $cm^{-1}$ due to the $\upsilon$(C═O) stretch and a broad band at 1280−1295 $cm^{-1}$ due to the $\upsilon$(C−O) stretch of the carboxylic acid groups. Extensive hydrogen bonding of the carboxylic acid groups in *p*-ZnTCPP-[A][24] resulted in a shift to lower frequency and broadening of the $\upsilon$(C═O) stretch at 1638 $cm^{-1}$ and a shift to higher frequency of the $\upsilon$(C−O) stretch at 1384 $cm^{-1}$. The differences observed between the spectra of the carboxylic acids and the triethylammonium salts correspond well with those observed between the spectra of benzoic acid and its triethylammonium salt (see the Supporting Information). Both *p*- and *m*-ZnTCPP-[S] showed new bands at 1564 and 1271 $cm^{-1}$ which were assigned to the asymmetric and symmetric $\upsilon(CO_2^-)$ stretching modes, respectively. For both *m*-$ZnTCP_2P$-[S] and *m*-ZnTC(PEP)P-[S] the asymmetric $\upsilon(CO_2^-)$ stretch was very broad and at slightly higher frequency, ∼1580 $cm^{-1}$. Their corresponding symmetric stretches were broadened and shifted to lower frequency, at ∼1260 $cm^{-1}$. For all triethylammonium salts there was an additional $\upsilon$(C═O) stretch at 1702 $cm^{-1}$ due to hydrogen bonding of the $Et_3N^+H$ proton with the carboxylate group.[25]

**3.2.2. Bound to $TiO_2$.** In the bound spectra of the meta-substituted tetraacid porphyrins (Figure 2) the $\upsilon$(C═O) and $\upsilon$(C−O) stretching modes disappear with the appearance of a broad shoulder on the high-frequency side of the phenyl breathing mode (1605−1740 $cm^{-1}$). For all four porphyrin acids and salts, binding to $TiO_2$ films resulted in the appearance of strong and broad bands in the 1390−1410 $cm^{-1}$ region, which are characteristic of the symmetric $\upsilon(CO_2^-)$ stretch. A broad band observed at ∼1540 $cm^{-1}$ for the porphyrin acids and salts bound to $TiO_2$ was assigned to the $\upsilon(CO_2^-)$ asymmetric stretching mode. Overall, the spectral changes, both for porphyrin acids/$TiO_2$ and salts/$TiO_2$, are consistent with chelating and/or bidentate binding modes of the carboxylate groups on the $TiO_2$ surface (Figure 3).[26]

This is also confirmed by a decrease in the difference between the symmetric and asymmetric bands of the carboxylate group of the salt derivatives ($\Delta \sim 290$ $cm^{-1}$) on binding to $TiO_2$ ($\Delta \sim 240$ $cm^{-1}$).[26] A number of $\upsilon$(C═O) stretching modes were still evident for *p*-ZnTCPP-[A] on $TiO_2$ indicating the presence of free carboxylic acid groups for this sensitizer (Figure 4). The weak acetylenic $\upsilon$(C≡C) stretch was observed from 2215 to 2233 $cm^{-1}$ for all of the *m*-ZnTC(PEP)P derivatives. The characteristic $N^+-H$ bending mode of the triethylammonium counterion is observed in the 2850−2950 $cm^{-1}$ region for all salt derivatives.[25]

**3.3. UV−Vis Absorption and Fluorescence Emission Spectra. 3.3.1. Solution.** Table 1 summarizes the solution absorption and emission data for the $COOEt_3NH$ derivatives of all four porphyrins in methanol. The UV−vis absorption and fluorescence emission spectra in fluid solutions of all derivatives (COOH, COOMe, and $COOEt_3NH$) of the zinc porphyrins were similar. Also, neither the substitution position (para vs meta), nor the length of the rigid spacer between the porphyrin ring and the carboxy groups, caused any significant shift in their absorption or emission maxima (Table 1).

All solution UV−vis absorption spectra exhibited the features typical of the ZnTPP ring, with absorptions at ∼424 nm (the "Soret" band, corresponding to the $S_0 \rightarrow S_2$ transition) and at ∼558 and ∼597 nm (the "Q bands", corresponding to the higher vibrational mode Q(1,0) and the lowest energy vibrational mode Q(0,0) of the $S_0 \rightarrow S_1$ transition). Figure 5a shows an overlay of the UV−vis spectra of the $COOEt_3NH$ derivatives for all four porphyrins recorded in MeOH.

The similarities observed in the solution absorption spectra of all porphyrins here studied are attributed to the lack of electronic communication between the *meso*-aryl substituents and the porphyrin ring. In this respect, *p*-ZnTCPP, *m*-ZnTCPP, *m*-$ZnTCP_2P$, and *m*-ZnTC(PEP)P are good models to determine the effect of binding orientation and sensitizer distance without significantly changing the electronic properties of the porphyrin ring. However, the rotational barrier of the *o*-H-substituted *meso*-aryl substituents is low.[10c,27] For *meso*-aryl substituents having bulkier groups in the ortho position, atropisomers are typically observed.[28] No atropisomers were observed for any porphyrins synthesized in this study. The solution fluorescence emission spectra of the four porphyrin ammonium salts *p*-ZnTCPP-[S], *m*-ZnTCPP-[S], *m*-$ZnTCP_2P$-[S], and *m*-ZnTC(PEP)P-[S] were also typical of tetra-aryl Zn(II)porphyrin systems and showed almost identical $\lambda_{max}$ in their spectra (Figure 5b).

**3.3.2. Bound to $TiO_2$, ZnO, and $ZrO_2$ Films.** Both the tetracarboxylic acid and tetra(triethylammonium)salt derivatives

(23) (a) Thomas, D. W.; Martell, A. E. *J. Am. Chem. Soc.* **1959**, *81*, 5111. (b) Datta-Gupta, N.; Bardos, T. J. *J. Heterocycl. Chem.* **1966**, *3*, 495. (c) Longo, F. R.; Finarelli, M. G.; Kim, J. B. *J. Heterocycl. Chem.* **1969**, *6*, 927.
(24) Diskin-Posner, Y.; Goldberg, I. *Chem. Commun.* **1999**, 1961.
(25) Odinokov, S. E.; Glazunov, V. P.; Nabiullun, *J. Chem. Soc., Faraday Trans. 2* **1984**, *80*, 899.
(26) (a) Deacon, G. B.; Phillips, R. J. *Coord. Chem. Rev.* **1980**, *33*, 227. (b) Finnie, K. S.; Bartlett, J. R.; Woolfrey, J. L. *Langmuir* **1998**, *14*, 2744. (c) Vittadini, A.; Selloni, A.; Rotzinger, F. P.; Grätzel, M. *J. Phys. Chem. B* **2000**, *104*, 1300. (d) Nazeeruddin, M. K.; Humphrey-Baker, R.; Liska, P.; Grätzel, M. *J. Phys. Chem. B* **2003**, *107*, 8981.
(27) (a) Eaton, S. S.; Eaton, G. R. *J. Am. Chem. Soc.* **1975**, *97*, 3660. (b) Eaton, S. S.; Eaton, G. R. *J. Am. Chem. Soc.* **1977**, *99*, 6594. (c) Eaton, S. S.; Fishwild, D. M.; Eaton, G. R. *Inorg. Chem.* **1978**, *17*, 1542. (d) Stolzenberg, A. M.; Haymond, G. S. *Inorg. Chem.* **2002**, *41*, 30. (e) Medforth, C. J.; Haddad, R. E.; Muzzi, C. M.; Dooley, N. R.; Jaquinod, L.; Shyr, D. C.; Nurco, D. J.; Olmstead, M. M.; Smith, K. M.; Ma, J.-G.; Shelnutt, J. A. *Inorg. Chem.* **2003**, *42*, 2227. (f) Ayabe, M.; Yamashita, K.; Sada, K.; Shinkai, S.; Ikeda, A.; Sakamoto, S.; Yamaguchi, K. *J. Org. Chem.* **2003**, *68*, 1059. (g) Tong, L. H.; Pascu, S. I.; Jarrosson, T.; Sanders, J. K. M. *Chem. Commun.* **2006**, 1085
(28) Freitag, R.; Whitten, D. G. *J. Phys. Chem.* **1983**, *87*, 3918.

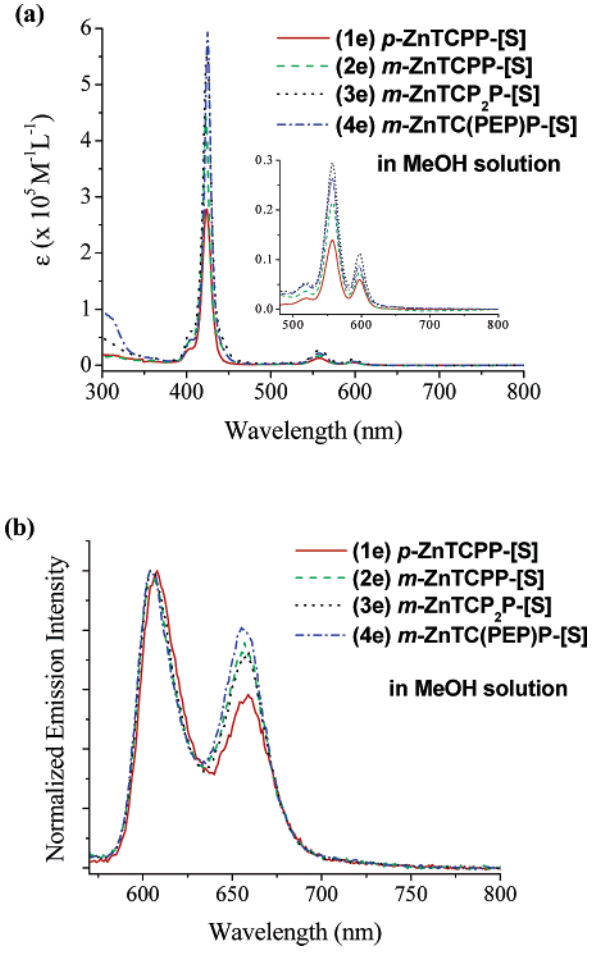


***Figure 5.*** Solution (a) UV−vis absorption spectra and (b) fluorescence emission spectra of tetra(triethylammonium)carboxyporphyrin salts recorded in methanol.

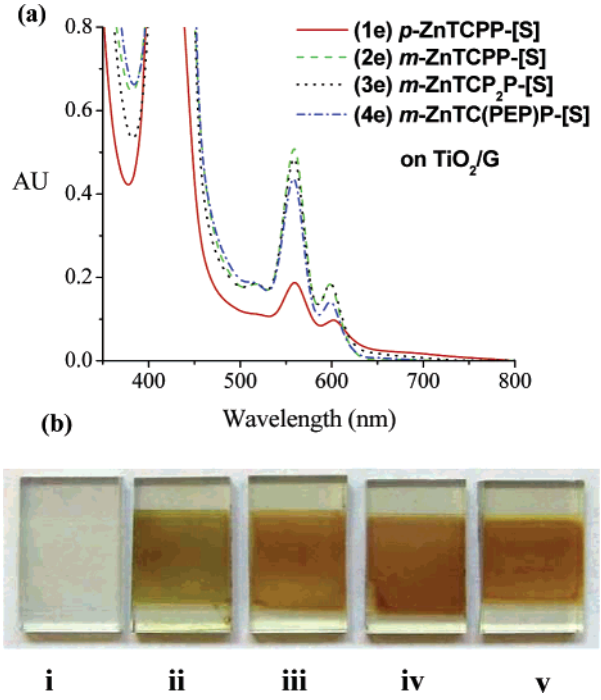


***Figure 6.*** (a) UV−vis absorption spectra of tetra(triethylammonium)-carboxyporphyrin salts on $TiO_2$/G. Comparable UV−vis absorption spectra were observed for all sensitizers on $TiO_2$ and $ZrO_2$ mesoporous films. (b) Picture of (i) blank $TiO_2$/ITO, (ii) *p*-ZnTCPP-[A], (iii) *m*-ZnTCPP-[A], (iv) *m*-$ZnTCP_2P$-[A], and (v) *m*-ZnTC(PEP)-[A] bound to $TiO_2$/ITO films. Note the difference in color between the *p*-ZnTCPP-[S] film and the meta-substituted systems.

for all four porphyrins were found to bind efficiently to $TiO_2$, ZnO,[29] and $ZrO_2$ nanoparticle films. Because of the wider band gap, $ZrO_2$ behaves as an insulator precluding electron injection from the lowest excited-state of all porphyrins studied here ($E_{bg}$ ~ 5 eV for $ZrO_2$ compared to ~3 eV for $TiO_2$ and ZnO). Since the fluorescence is not quenched, the $ZrO_2$ films are an excellent substrate to study the fluorescence emission of the porphyrins bound to a surface that closely resembles the morphology of $TiO_2$ films. Significant differences in the absorption and emission spectra were observed between the para and meta porphyrin systems (acids or salts). The UV−vis absorption spectra of the triethylammonium salts bound to $TiO_2$ are shown in Figure 6.

Comparable UV−vis absorption spectra were observed for all porphyrins (acids or salts) on $TiO_2$ and $ZrO_2$ mesoporous films. The thicker (~10 $\mu$m) $TiO_2$ and $ZrO_2$ films had a greater absorption when compared to that of the thinner ZnO films (~2 $\mu$m). The Soret absorption, which was very intense on $TiO_2$ and $ZrO_2$ films, was less intense on ZnO (Figures 6 and 7).

The most notable feature in the absorption spectra on ZnO films was the blue shift (10 nm) and splitting ($\lambda_{max}$ = 420 and 430 nm) of the Soret band for the para porphyrin *p*-ZnTCPP (acid or salt). Such behavior is indicative of exciton interaction between porphyrin chromophores, and previous studies on $TiO_2$ nanoparticles attributed this effect to the formation of H-aggregates (face-to-face stacking) between porphyrin molecules.[30] A small red shift (3 nm, $\lambda_{max}$ = 601 nm) and broadening of the lower energy Q(0,0) band was observed for the *p*-ZnTCPP acid or salt derivative bound to $TiO_2$, in comparison to the meta porphyrin acids or salts ($\lambda_{max}$ = 598 nm), which are expected to bind flat on $TiO_2$.[9a,31]

The fluorescence spectra of the meta porphyrin salts bound to $ZrO_2$, presumably with a planar binding mode, showed little deviation from their solution-phase spectra. However, the para-substituted porphyrin *p*-ZnTCPP (acid or salt) on $ZrO_2$, displayed broadening and convergence of the two porphyrin fluorescence bands (Figure 8). We attributed this effect to the formation of H-aggregates of the porphyrin ring on the $ZrO_2$ surface.

**3.4. Surface Coverage.** Coverage of the tetra(triethylammonium)carboxyporphyrin salts, calculated on the $TiO_2$ mesoporous films, decreased with the increasing length of the spacer: *m*-ZnTCPP-[S] (20 $\mu$mol $g^{-1}$) > *m*-$ZnTCP_2P$-[S] (19 $\mu$mol $g^{-1}$) > *m*-ZnTTC(PEP)P-[S] (12 $\mu$mol $g^{-1}$). The highest value was obtained for *p*-ZnTCPP-[S] (27 $\mu$mol $g^{-1}$) consistent with a closer packing in the para porphyrin, for which the "vertical" binding mode is proposed. The value reported here for *p*-

(29) The IPCE study was done on $TiO_2$ films. A photoelectrochemical study of *m*-ZnTCPP-[A] bound to ZnO nanorods has been previously reported, and similar studies for all porphyrins here described are forthcoming.

(30) Aratani, N.; Osuka, N.; Cho, H. S.; Kim, D. *J. Photochem. Photobiol., C* **2002**, *3*, 25.

(31) There is some precedent in the literature supporting the planar orientation of meta-substituted tetraphenylporphyrins on various surfaces, see: (a) Skupin, M.; Li, G.; Fudickar, W.; Zimmerman, J.; Röder, B.; Fuhrhop, J.-H. *J. Am. Chem. Soc.* **2001**, *123*, 3454. (b) Li, G.; Doblhofer, K.; Fuhrhop, J.-H. *Angew. Chem., Int. Ed.* **2002**, *41*, 2730. (c) Bhosale, S.; Li, G.; Li, F.; Wang, T.; Ludwig, R.; Emmler, T.; Buntkowsky, G.; Fuhrhop, J.-H. *Chem. Commun.* **2005**, 3559.

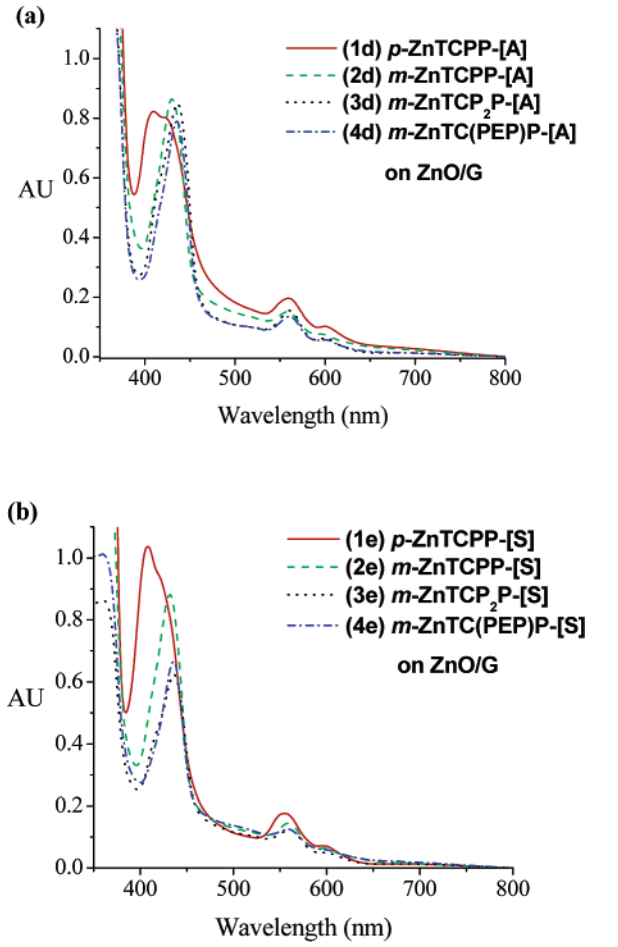


***Figure 7.*** UV−vis absorption spectra on mesoporous ZnO/G films of the (a) COOH derivatives and (b) $COO^{-}Et_3NH^{+}$ derivatives for all four porphyrins.

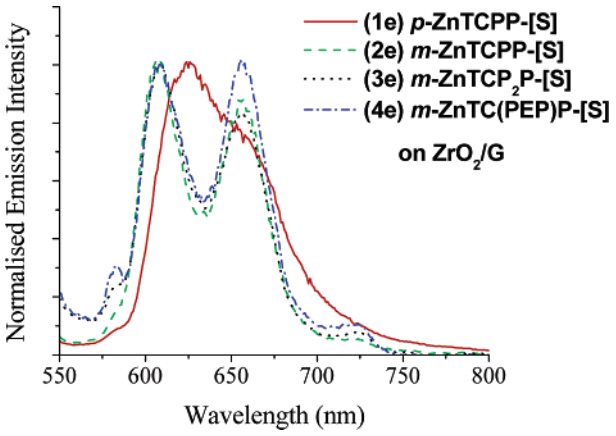


***Figure 8.*** Fluorescence emission spectra of tetra(triethylammonium)-carboxyporphyrin salts on $ZrO_2$/G.

ZnTCPP-[S] is lower than that previously reported by Cherian and Wamser[32] for *p*-ZnTCPP-[A] (47 $\mu$mol $g^{-1}$). However, that value described the saturation coverage of the mesoporous $TiO_2$ film after binding overnight, whereas the binding times in our experiments were much shorter (1 h). Variations in film thickness and nanoparticle size, commonly observed from laboratory to laboratory, could also lead to such differences. The trend observed here in the coverage is what would be

(32) Cherian, S.; Wamser, C. C. *J. Phys. Chem. B* **2000**, *104*, 3624.

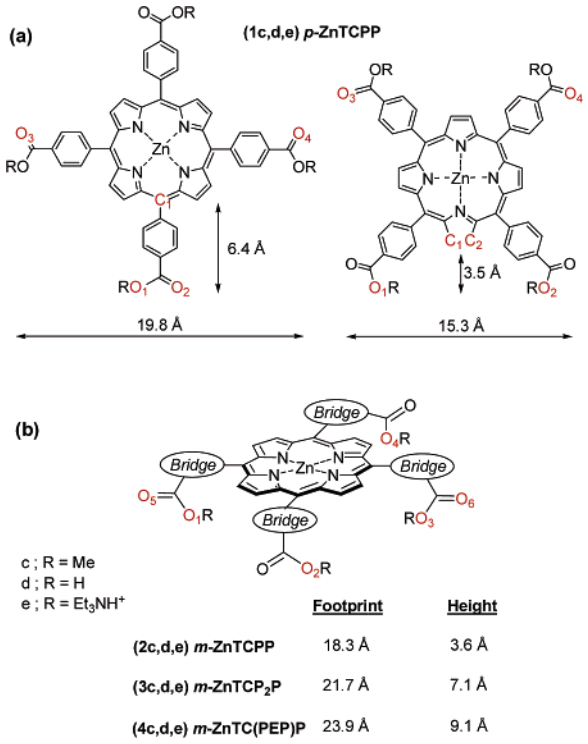


***Figure 9.*** Calculated molecular dimensions of (a) *p*-TCPP and (b) *m*-ZnTCPP, *m*-$ZnTCP_2P$, and *m*-ZnTC(PEP) (ref 33).

***Table 2.*** Solution Redox Potentials of Tetramethylester Porphyrins in Dichloromethane Reported versus NHE (V)[a]

| | oxidation (V) | | reduction (V) | | | | |
|---|---|---|---|---|---|---|---|
| porphyrin | 1st | 2nd | 1st | 2nd | 3rd[b] | $E_{0-0}$ (eV) | $E_{1/2}(P^{+}/P^{*})$ (eV) |
| (1c) *p*-ZnTCPP-[E] | 1.10 | 1.47 | −1.12 | −1.46 | −1.64 | 2.06 | −1.04 |
| (2c) *m*-ZnTCPP-[E] | 1.11 | 1.38 | −1.08 | −1.45 | | 2.07 | −1.04 |
| (3c) *m*-ZnTCP2P-[E] | 1.12 | 1.37 | −1.08 | −1.31 | −1.46 | 2.07 | −1.05 |
| (4c) *m*-ZnTC(PEP)P-[E] | 1.11 | 1.38 | −1.09 | −1.33 | −1.46 | 2.07 | −1.04 |

[a] All cyclic voltammograms were measured at a scan rate of 100 mV $s^{-1}$ using a glassy carbon working electrode. [b] Determined from differential pulse voltammetry experiments.

expected considering the size (Figure 9) and anticipated binding geometry ("flat" vs "vertical") of each sensitizer (Figure 1). A lower surface coverage would be expected with increasing footprint size of the sensitizer (Figure 9). Also, larger molecules may not penetrate the smaller pores in the $TiO_2$ film.

**3.5. Electrochemical Properties. 3.5.1. Solution.** Table 2 lists the solution redox potentials of tetramethylester porphyrins *p*-ZnTCPP-[E], *m*-ZnTCPP-[E], *m*-$ZnTCP_2P$-[E], and *m*-ZnTC-(PEP)P-[E] reported versus NHE. The solution electrochemical measurements were performed on the methylester derivatives, because the acid or ammonium salt derivatives were insoluble in dichloromethane. All compounds exhibited redox behavior typical of Zn(II)TPP porphyrins (Table 2).

Two reversible oxidation processes were observed due to the formation of the porphyrin radical cation and the diradical cation

(33) For *p*-TCPP with one bound carboxyl group the approximate height from the $TiO_2$ surface was taken as the distance from $C_1$ to the midpoint of $O_1$ and $O_2$ and the diameter as the distance from $O_3$ to $O_4$. For *p*-TCPP with two bound carboxyl groups, the approximate height from the $TiO_2$ surface was taken as the distance from the midpoint of $C_1$ and $C_2$ to the midpoint of $O_1$ and $O_2$ and the diameter as the distance from $O_3$ to $O_4$. For the meta-substituted porphyrins the height was taken as the distance from the plane of the porphyrin to the plane defined by the four oxygens $O_1$−$O_4$. The footprint diameter was calculated as the distance from $O_5$ to $O_6$. Modeling was done using Spartan '02 modeling software, Wavefunction, Inc.

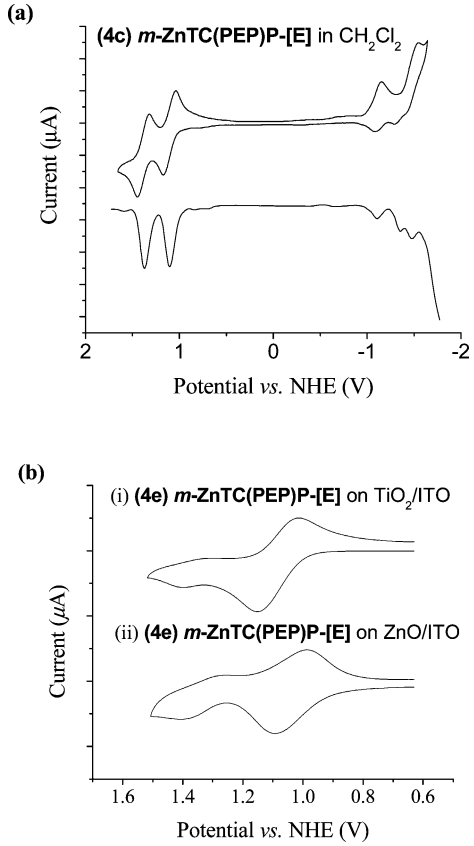


***Figure 10.*** (a) Solution ($CH_2Cl_2$) cyclic voltammogram (i) and differential pulse voltammogram (ii) scans of *m*-ZnTC(PEP)P-[E]. (b) Cyclic voltammogram scans of *m*-ZnTC(PEP)P-[S] bound to (i) $TiO_2$/ITO and (ii) ZnO/ITO electrodes.

species, respectively. In the negative potential region three quasi-reversible reduction processes were observed.[34] The first reduction process, observed in the range of −1.08 to −1.12 V versus NHE, is attributed to the reduction of the low-lying LUMO orbital of the carboxy moieties. The second and third reduction processes are attributed to the reversible formation of the porphyrin radical anion and diradical anion species, respectively.[35] Only two reduction processes were observed for *m*-ZnTCPP-[E], and it is possible that the formation of the diradical anion species of this compound occurs outside the potential window under the conditions employed. Cyclic voltammetry and differential pulse voltammetry scans for *m*-ZnTC(PEP)P-[E] are shown in Figure 10a.

**3.5.2. Bound to $TiO_2$ and ZnO.** Analogous to the solution studies, a reversible first oxidation was observed in the range of +1.09 to +1.10 V versus NHE on $TiO_2$ and +1.04 to +1.07 V versus NHE on ZnO surfaces, due to the formation of the porphyrin radical cation species. Formation of the diradical cationic species was irreversible on both $TiO_2$ and ZnO surfaces. For DSSCs applications, the stability of the sensitizer is dependent on the reversibility of the first oxidation process following charge injection into the metal oxide semiconductor from the photoexcited chromophore. Table 3 summarizes the redox behavior of *p*-ZnTCPP-[E], *m*-ZnTCPP-[E], *m*-$ZnTCP_2$P-[E], and *m*-ZnTC(PEP)P-[E] bound to both $TiO_2$/ITO and ZnO/ITO mesoporous thin films.

***Table 3.*** Redox Potentials of Tetra(triethylammonium)carboxyporphyrin Salts Bound to $TiO_2$/ITO and ZnO/ITO Films versus NHE (V)[a]

| | $TiO_2$/ITO (V) | | | | ZnO/ITO (V) | | | |
|---|---|---|---|---|---|---|---|---|
| porphyrin | 1st | 2nd[b] | $E_{0-0}$ (eV) | $E_{1/2}(P^+/P^*)$ (eV) | 1st | 2nd[b] | $E_{0-0}$ (eV) | $E_{1/2}(P^+/P^*)$ (eV) |
| (1e) *p*-ZnTCPP-[S] | 1.09 | 1.38 | 2.03 | −1.06 | 1.07 | 1.43 | 2.03 | −1.04 |
| (2e) *m*-ZnTCPP-[S] | 1.10 | 1.36 | 2.06 | −1.04 | 1.06 | 1.42 | 2.06 | −1.00 |
| (3e) *m*-ZnTCP2P-[S] | 1.09 | 1.35 | 2.06 | −1.03 | 1.07 | 1.42 | 2.05 | −1.02 |
| (4e) *m*-ZnTC (PEP)P-[S] | 1.10 | 1.36 | 2.06 | −1.04 | 1.04 | 1.41 | 2.05 | −0.99 |

[a] All samples were run at a scan rate of 100 mV $s^{-1}$ using the derivatized MO/ITO films as the working electrode. [b] Anodic peak maxima ($E_{pa}$).

Cyclic voltammetry scans for *m*-ZnTC(PEP)P-[S] bound to $TiO_2$/ITO and ZnO/ITO working electrodes are shown in Figure 10b. The oxidation of sensitizers bound to wide band gap semiconductors, such as $TiO_2$, has been explained by an electron−hole transfer process which permeates through the adsorbed layer of dye.[36] According to this mechanism, the molecules closest to the conducting glass are oxidized, and the adjacent dye molecules are then oxidized via electron−hole transfer. The large peak width observed for *m*-ZnTC(PEP)P-[S] bound to $TiO_2$/ITO or ZnO/ITO working electrodes (∼200 mV at half-height) was typical for all compounds and is most probably due to a slight dispersion in the redox potentials caused by inhomogeneities of the films. $E_{1/2}(P^+/P^*)$ is an important value to consider when designing a chromophore for DSSCs, as it determines the driving force for electron transfer to the lower-lying conduction band of the semiconductor. The excited-state oxidation potential of all porphyrins here studied was about −1 V versus NHE, which is quite negative with respect to the conduction bands of both the $TiO_2$[37] and ZnO[38] semiconductors. In summary, these porphyrins are good photoreductants. A comparison between the $E_{1/2}(P^+/P^*)$ values in solution and bound showed a slight increase in the excited-state oxidation potential for *p*-ZnTCPP-[S]. This effect was once again attributed to aggregation at the metal oxide surface for the para porphyrin and was not observed for the meta porphyrins.

**3.6. Photoelectrochemical Measurements in DSSCs.** The main objective of the photoelectrochemical experiments was to determine the effect of the binding geometries of the sensitizer on the solar cell efficiencies. The photocurrent action spectra of all four triethylammonium porphyrin salts bound to $TiO_2$/FTO are shown in Figure 11.

The photocurrent action spectra of all sensitizers concurred reasonably well with their corresponding absorption spectra. The IPCE for *m*-ZnTCPP-[S] at 430 nm (59%), corresponding to the Soret absorption band, represented a 3-fold increase with respect to the para-substituted analogue *p*-ZnTCPP-[S] at the corresponding wavelength. IPCE values at the lower energy Q bands of *m*-ZnTCPP-[S] and *m*-$ZnTCP_2$P-[S] were in the range of 16−34%, which is a greater than 20-fold increase with respect to the IPCE values observed in the same region for *p*-ZnTCPP-[S] (Table 4).

For all porphyrins, the Soret band showed the highest IPCE value. This was expected as its extinction coefficient is 1 order

(34) Wolberg, A.; Manassen, J. *J. Am. Chem. Soc.* **1970**, *92*, 2982.
(35) Clack, D. W.; Hush, N. S. *J. Am. Chem. Soc.* **1965**, *87*, 4238.
(36) Bonhote, P.; Gogniat, E.; Tingry, S.; Barbe, C.; Vlachopoulos, N.; Lenzmann, F.; Compte, P.; Grätzel, M. *J. Phys. Chem. B* **1998**, *102*, 1498.
(37) Liu, G.; Jaegermann, W.; He, J.; Sündstrom, V.; Sun, L. *J. Phys. Chem. B* **2002**, *106*. 5814.
(38) Redmond, R.; O'Keeffe, A.; Burgess, C.; MacHale, C.; Fitzmaurice, D. *J. Phys. Chem.* **1997**, *97*, 11081.

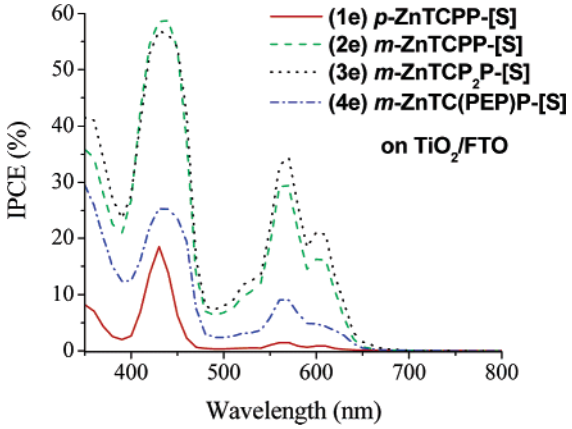


***Figure 11.*** Photocurrent action spectra of tetra(triethylammonium)-carboxyporphyrin salts.

***Table 4.*** Photoelectrochemical Properties of Tetra(triethylammonium)carboxyporphyrin Salts

| | | | | IPCE (%) | | |
|---|---|---|---|---|---|---|
| porphyrin | $I_{sc}$ (mA cm$^{-2}$) | $V_{oc}$ (V) | *ff* | 430 nm | 570 nm[a] | 600 nm[b] |
| (1e) *p*-ZnTCPP-[S] | 0.39 | 0.44 | 0.54 | 18.50 | 1.44 (0.08) | 0.86 (0.05) |
| (2e) *m*-ZnTCPP-[S] | 3.33 | 0.51 | 0.41 | 58.60 | 29.40 (0.50) | 16.30 (0.28) |
| (3e) *m*-ZnTCP2P-[S] | 3.72 | 0.50 | 0.42 | 56.90 | 34.50 (0.61) | 21.10 (0.37) |
| (4e) *m*-ZnTC(PEP)P-[S] | 1.36 | 0.43 | 0.45 | 25.30 | 9.00 (0.36) | 4.81 (0.19) |

[a] In parentheses are the Q(1,0) vs Soret peak intensity ratios. [b] In parentheses are the Q(0,0) vs Soret peak intensity ratios.

of magnitude larger than for the Q bands. However, the larger increase in IPCE observed for the meta-substituted systems in the Q-band region, relative to the Soret absorption, suggests that the lower energy $S_1$ transition of the porphyrin chromophore has a greater quantum efficiency for charge injection when oriented in a planar geometry with respect to the $TiO_2$ surface. Q(1,0)/Soret peak intensity ratios of 0.08, 0.50, 0.61, and 0.36 were observed for the sensitizers *p*-ZnTCPP-[S], *m*-ZnTCPP-[S], *m*-ZnTCP$_2$P-[S], and *m*-ZnTC(PEP)P-[S], respectively. The IPCE can also be expressed in terms of the light harvesting efficiency (LHE), the quantum yield of charge injection ($\phi_{inj}$), and the charge collection efficiency at the back electrode ($\eta_c$) in eq 5

$$\text{IPCE} = (\text{LHE})\phi_{inj}\eta_c \qquad (5)$$

where $\eta_c$ is dependent upon both the rate of dye regeneration by the oxidation of electrolyte and the rate of charge recombination from the reduced $TiO_2$ particles to the oxidized sensitizer. According to the extinction coefficients and binding efficiencies calculated for all four sensitizers, and assuming equivalent values for $\phi_{inj}$ and $\eta_c$, this equation predicts only a slight increase in IPCE for the meta-substituted systems. Considering the comparable solution photophysical properties of all four sensitizers, and their similar ground and excited-state redox behavior, such large increases in the IPCE values was rationalized in terms of greater $\phi_{inj}$ for the porphyrin chromophore when oriented in a planar geometry. This interpretation is consistent with that made by Campbell et al. when they observed a 5-fold increase in $I_{sc}$ for *m*-ZnTCPP-[A] with respect to that of *p*-ZnTCPP-[A].[9a] Although little increase of $V_{oc}$ was observed for the meta-substituted systems,[39] a 3-, 8-, and 9-fold increase in $I_{sc}$ was observed for *m*-ZnTC(PEP)P-[S], *m*-ZnTCPP-[S], and *m*-ZnTCP$_2$P-[S], respectively, in comparison to that of the para-substituted *p*-ZnTCPP-[S]. The higher IPCE values observed for *m*-ZnTCP$_2$P-[S] in the Q-band region in comparison to those of *m*-ZnTCPP-[S] as well as its greater $I_{sc}$ suggest a reduced charge recombination for this system, possibly because of the increased distance of the porphyrin ring from the $TiO_2$ surface (Figure 9) and/or a better surface coverage blocking the electrons in the $TiO_2$ from reacting with the electrolyte. The lack of any aggregate absorption band in the photocurrent action spectrum of *p*-ZnTCPP-[S] suggests that aggregates do not contribute to any current generation.

(39) For an effect of dye distance on $V_{oc}$ see, for instance, ref 6d.

## 4. Conclusions

Four *para*- and *meta*-Zn(II) tetra(carboxyphenyl)porphyrins were studied in solution and bound to metal oxide ($TiO_2$, ZnO, and $ZrO_2$) nanoparticle films to determine the effect of the spacer length and anchoring group position on their photoelectrochemical and photophysical properties. Both COOH and COOEt$_3$NH derivatives were employed for the binding studies as well as solution studies. Solution phase electrochemistry studies were performed on the methyl ester derivatives (COOMe). In *m*-ZnTCPP, *m*-ZnTCP$_2$P, and *m*-ZnTC(PEP)P the anchoring groups are in meta position on the *meso*-phenyl rings. The meta substitution favored a planar binding mode to the metal oxide surfaces, as determined by a combination of studies that included IR, UV, and solar cell efficiencies on $TiO_2$. Fluorescence emission was studied on $ZrO_2$. All studies indicated that only *p*-ZnTCPP aggregated, suggesting close packing of the dye molecules on the semiconductor surface. Aggregation effects were not observed for the meta porphyrins. These observations are consistent with the work of others on *p*-ZnTCPP and *m*-ZnTCPP. The photoelectrochemical behavior of the para- and meta-substituted porphyrin sensitizers suggests that the binding geometry, as well as the distance of the sensitizer from the metal oxide surface, dramatically influence their efficiencies. The greater efficiency of the rigid planar meta-substituted systems was explained in terms of a greater charge injection into the $TiO_2$ semiconductor from rings that lie flat, and closer, to the surface. A kinetic study of the injection and recombination processes for all four compounds described here is clearly of interest, and this work is forthcoming.

**Acknowledgment.** E.G. thanks DOE (DE-FG02-01ER15256) for funding. J.R. and E.G. thank the Rutgers Research Council for travel funds. D.C. thanks the OISE office of NSF for an REU supplement (NIRT-0303829) for an undergraduate summer stipend and international travel funds. E.G. thanks Professor Mendelsohn for generously making available IR instrumentation. D.C. thanks Dr. Häggman, Dr. Edvinsson, and Dr. Boschloo for help with the solar cell measurements.

**Supporting Information Available:** Preparation of the $TiO_2$ and $ZrO_2$ films; $TiO_2$ Raman, PXRD, and AFM data; *p*-H$_2$-TCPP-[E], *m*-H$_2$TCPP-[E], *p*-ZnTCPP-[E], *m*-ZnTCPP-[E], *p*-ZnTCPP-[A], and *m*-ZnTCPP-[A] NMR data; FT-IR-ATR spectra of **1d** and **e**, **2d** and **e**, **3d** and **e** neat and bound to $TiO_2$. This material is available free of charge via the Internet at http://pubs.acs.org.

JA068218U